ISSN 1392–1320 MATERIALS SCIENCE (MEDŽIAGOTYRA). Vol. 21, No. 3. 2015

# The Electrical and Microstructural Properties of Zr-doped $LaNbO_4$ Thin Ceramic Films

**Darius VIRBUKAS, Kristina BOČKUTĖ, Giedrius LAUKAITIS***

*Physics Department, Kaunas University of Technology, Studentu str. 50, LT-51368 Kaunas, Lithuania*

crossref http://dx.doi.org/10.5755/j01.ms.21.3.9535

*Received 19 January 2015; accepted 11 April 2015*

In the current research thin Zr-doped lanthanum niobium oxide ($LaNb_{1-x}Zr_xO_4$) films deposited by magnetron sputtering were studied to investigate their microstructural and electrical properties. The main attention is paid to the electrical processes in the formed thin films, e.g. relaxation time and activation energy derived from the different electrical parameters. X-ray diffractometry, energy-dispersive X-ray spectroscopy and scanning electron microscopy were used to study the structure and composition of the films. Electrical parameters of $LaNb_{1-x}Zr_xO_4$ thin ceramic were investigated by impedance spectroscopy in the frequency range from 0.1 Hz to 1.0 MHz in temperature range from 773 to 1173 K. It is shown that $LaNb_{1-x}Zr_xO_4$ thin ceramic films have nanocrystalline structure with characteristic peaks corresponding to the tetragonal $LaNbO_4$ structure. The increase of Zr dopants does not influence the tetragonal structure. It was revealed that the Non-Debye relaxation process is dominant in the formed thin films and the activation energy is dependent on the concentration of the dopants. The comparison between the activation energies estimated using different electrical parameters: electrical modulus, impedance imaginary part and slope from the conductivity plot was made. Also the relaxation time was calculated. The relaxation time varies from from $2.80 \cdot 10^{-4}$ s to $3.78 \cdot 10^{-5}$ s in the formed thin films.
*Keywords:* Complex electrochemical impedance spectroscopy, magnetron sputtering, thin films, $LaNbO_4$.

## 1. INTRODUCTION

Lanthanoides orthoniobates are promising materials for multiple applications. They are ferroelastic, have excellent microwave dielectric properties, also they can be characterized as good luminescent materials [1 – 4]. Doped lanthanum niobates are used as transparent electro-optical materials [5]. Moreover, their application as protonic conductors has attracted a lot attention in the recent years [6 – 10]. In addition, the purity of proton conductivity makes this class of materials interesting for hydrogen and humidity sensors at temperatures below 700 °C. In order to improve the proton conductivity in lanthanum niobates the doping with lower valence elements, thus the generation of the oxygen vacancies, is necessary. Usually, lanthanum is replaced by calcium or magnesium dopants and niobium is replaced by titanium, zirconium or indium dopants [9, 11, 12, 13]. The doping of the lanthanum niobates has the influence on the mechanical and thermal properties as well. Doped lanthanum niobates exhibit more uniform surface and the size of the grains and crystallites is reduced also [14]. Doped lanthanum niobates can exhibit different structural, optical and electrochemical properties [6 – 13]. In general these properties are dependent on the formation method and type of the dopant. Meanwhile the magnetron sputtering is not investigated for the formation of the doped $LaNbO_4$ at all and there is a lack of the studies to analyse the influence of the dopants replacing niobium in the $LaNbO_4$ lattice. Therefore the aim of this research is to investigate the influence of the Zr dopants on the electrical and microstructural properties of the $LaNbO_4$ thin films deposited using magnetron sputtering paying attention to the electrical processes in the formed thin films, e.g. relaxation time and activation energy derived using different methods.

## 2. EXPERIMENTAL DETAILS

Lanthanum niobium oxide ($LaNbO_4$) thin films were grown on the optical quartz ($SiO_2$) substrates using magnetron sputtering technique. Substrates were prepared using the traditional methods [15] and the surface was treated in Ar gas at radio frequency (RF) ion plasma for 10 min. before deposition. RF plasma power was 100W. The deposition rate for the formation of thin $LaNbO_4$ films was fixed.

The thin films were formed on the substrates at 573 K temperature. In order to get the surface homogeneity, the substrates were rotated at constant 8 rpm speed. The thickness of the formed thin films was 1.4 μm. Three magnetrons system with La (pulsed 150 kHz), Nb (DC) and Zr (DC) cathodes was used to form Zr-doped lanthanum niobates thin films. To ensure the oxidic nature of the formed thin films, the deposition was done in Ar (30 sccm) and $O_2$ (6 sccm) gas environment. The used powers are presented in the Table 1.

The characterization of the formed thin films thickness profilometer (Ambios Technology XP-200) was employed. X-ray diffraction (XRD) data were collected at room temperature with D8 Discover (Bruker AXS GmbH) diffractometer using Cu $K_{\alpha 1}$ ($\lambda = 0.1540562$ nm) radiation. The crystal structures of thin ceramic films were analysed by the Scherrer's method using TOPAS software.

The microstructure of thin ceramic films was characterized by scanning electron microscopy (SEM) using a Hitachi S-3400N microscope.

* Corresponding author. Tel.: +370-37-300340; fax: +370-37-300302.
E-mail address: *giedrius.laukaitis@ktu.lt* (G. Laukaitis)

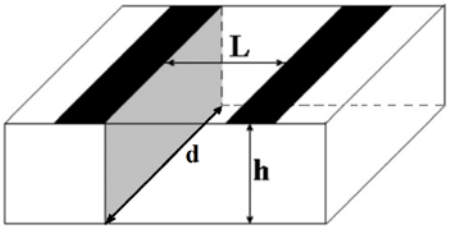


**Fig. 1.** Sample geometry for two electrode measurements

The electrochemical impedance spectroscopy measurements were performed in temperature range between 773 K and 1273 K with a 40 K step in air atmosphere. The data acquisition was done by ProboStat (NorECs AS) in a frequency range of $10^{-1} \leq f \leq 10^{6}$ Hz. The platinum electrodes were formed on the electrolyte before the measurements, and the impedance spectra were measured in-plane (Fig. 1), where *L* is the distance between electrodes, *d* is the length of the electrodes and *h* is the thickness of the thin film. The Pt electrodes (geometry 1.5 × 0.5 cm) were coated on a surface of the thin films before the measurement. The conductivity was calculated according to

$$\sigma = \frac{L}{AR}, \quad (1)$$

where *L* corresponds to the distance between electrodes, *A* is the cross-sectional area, and *R* is the resistance obtained from the impedance spectra [15].

The relaxation time (τ) of the thin ceramic films at different temperatures was calculated using the relation [16]:

$$\tau = \frac{1}{\omega} = \frac{1}{2\pi f_{max}}, \quad (2)$$

where $f_{max}$ is the frequency (the value of frequency at $Z''_{max}$ or $M''_{max}$).

## 3. RESULTS AND DISCUSSION

According to the EDS measurements, the power used for the deposition of the Zr dopant has the influence on the elemental composition of the formed thin films. It is seen that by increasing the Zr cathode power the concentration of the zirconium in the thin film increases (Table 1). The calculated La:Nb ratio in the thin films is equal to 0.98 indicating that the structure of the films is non-stoichiometric with the excess of niobium.

**Table 1.** Elemental composition of Zr-doped $LaNbO_4$ by changing Zr cathode power

| Power of magnetrons, W | | | Atomic concentration of Zr in thin film, at. % |
|---|---|---|---|
| $P_{La}$ | $P_{Nb}$ | $P_{Zr}$ | |
| 200 | 170 | 25 | 0.62 ± 0.01 |
| 200 | 170 | 33 | 1.14 ± 0.01 |
| 200 | 170 | 42 | 1.99 ± 0.01 |

The XRD diffraction pattern of the formed $LaNb_{1-x}Zr_xO_4$ thin ceramic film on optical quartz substrate is presented in Fig. 2. The non-stoichiometric structure of the formed thin films influenced the intensities of the XRD peaks but did not cause the appearance of the secondary phases in the $LaNbO_4$ structure. All visible Bragg peaks correspond to the tetragonal structure of $LaNbO_4$. The doping with different concentration of Zr dopants does not distort the tetragonal structure of $LaNbO_4$ (Fig. 2). Authors [17, 18] determined that the compounds of the $LaNbO_4$ are not following the Vegard's law and the structure is not distorted unless the concentration of the dopants is higher than 2 at. %. After overcoming this concentration the secondary phases are formed in the structure. Our results are in good agreement with the literature data [17, 18]. The size of the crystallites is increasing according to the Zr dopants' concentration and it is varying from 26.4 nm for the thin films with Zr concentration of 0.62 at. % to 44.7 nm for the thin films with Zr concentration of 1.99 at. %. In comparison, the crystallite size of the Ca-doped $LaNbO_4$ formed using spark plasma sintering was found to be in average 25 nm [19].

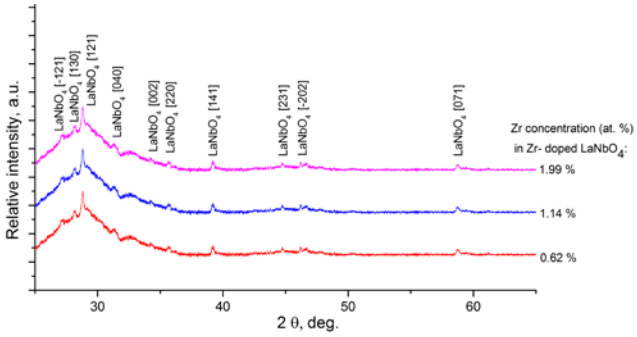


**Fig. 2.** XRD pattern of tetragonal phase of $LaNb_{1-x}Zr_xO_4$ thin ceramic film deposited on optical quartz

SEM images (Fig. 3) show that $LaNb_{1-x}Zr_xO_4$ thin ceramic films are homogenous and have columnar structure, which is without visible pores or cavities.

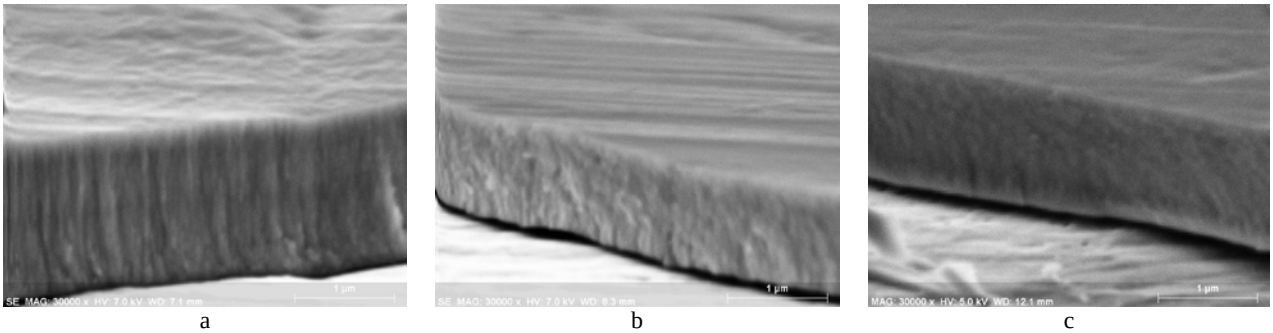

a b c

**Fig. 3.** SEM images of the cross-section of $LaNb_{1-x}Zr_xO_4$ thin ceramic films: a – 0.62 at. % Zr; b – 1.14 at. % Zr; c – 1.99 at. % Zr

The calculated relative density is 95 ± 2 % in average for all formed thin films.

The variation of real part (*Z*') of impedance with frequency at different temperatures (Fig. 4) shows the decrease in the values of *Z*'. The value of *Z*' decreases with increase in temperature in the low-frequency region. This character may be due to the release of space charge. This behaviour changes drastically in the high frequency region showing the complete merger of *Z*' plot. At high frequency, the *Z*' value at each temperature coincides implying the possible release of space charge [20].

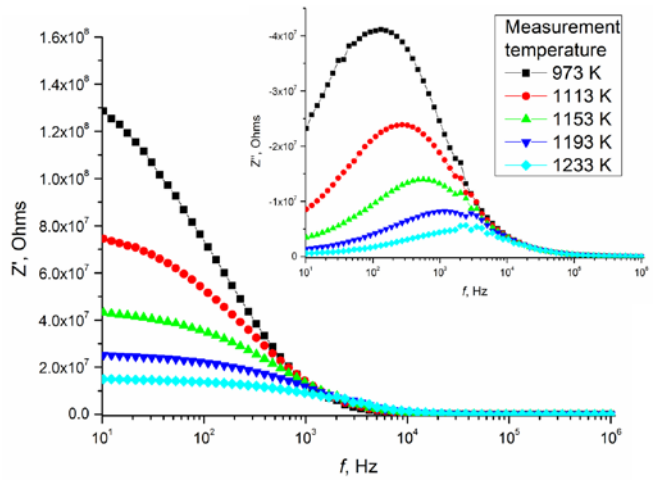


**Fig. 4.** Variation of real part (*Z*') of impedance with frequency at different temperature for the $LaNb_{1-x}Zr_xO_4$ (0.62 at. %) thin ceramic films. The inset shows the variation of imaginary part (*Z*'') of impedance with frequency at different temperature for the $LaNb_{1-x}Zr_xO_4$ (0.62 at. %) thin ceramic films

The peaks of the imaginary part (*Z*'') are of maximum value and shift to higher frequency range with increasing the temperature (Fig. 4 inset). This maximum value of the frequency is defined as the electrical relaxation frequency ($\omega_{max}$). The shift of the *Z*'' relaxation frequency to the higher frequency side, when the temperature is increasing, shows the increase of tangent loss and thermally activated dielectric relaxation process in the formed thin films. The relaxation time varies from $2.80 \cdot 10^{-4}$ s to $3.78 \cdot 10^{-5}$ s. In general the relaxation time represents the transition probabilities of the charge carriers along the conducting surface and typically it is temperature dependent.

The complex impedance spectra of $LaNb_{1-x}Zr_xO_4$ (Zr 0.62 at. %) thin films at different temperature are shown in Fig. 5. The impedance of the material is characterized by the formation of semicircular arcs whose pattern changes with changing temperature. Generally it is possible to see grain and grain boundary semicircles. In our case, the grain resistance is negligible compared to grain boundary resistance and therefore the grain semicircles in impedance plots are very small. The total resistance $R = R_b + R_{gb}$ was considered for the analysis.

The relaxation frequency ($\omega_{max}$) at different temperatures was obtained from Cole-Cole plot and it is seen that the relaxation frequency depends on the temperature. The relaxation frequency shifts to the higher frequency range with increasing temperature as in the other ceramics [21, 22].

The $LaNb_{1-x}Zr_xO_4$ ceramics have asymmetric or partially depressed semicircle (Fig. 5) and the solid lines show the fitting of the semicircles. For a Debye-type relaxation, the electrical loss modulus *M*'' should give a bell-shaped curve that peaks at $\omega_{max}\tau = 1$ and the Cole-Cole plots should represent the non-depressed semicircle. The semicircles were fitted using the equivalent circuit with one resistance and constant phase element (Fig. 5 inset). The depressed semicircles of the $LaNb_{1-x}Zr_xO_4$ ceramics are caused by the Non-Debye type of relaxation. The observed Non-Debye relaxation process appears due to the inhomogeneity in the structure of the formed thin films or the structural relaxations due to these inmoheneities [23].

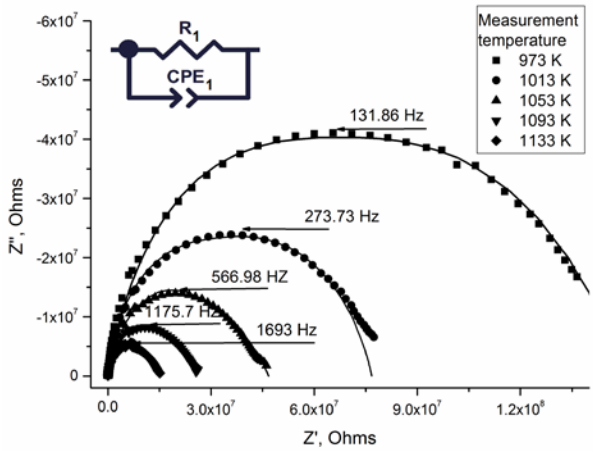


**Fig. 5.** Cole-Cole plot and equivalent circuit at different temperatures for the $LaNb_{1-x}Zr_xO_4$ (Zr 0.62 at. %) thin ceramic films. The solid line indicates the fitting.

The frequency dependence of *M*' and *M*'' were plotted in Fig. 6 for various temperatures. The peaks of *M*'' shift to higher frequencies as temperature increases. The frequency ($f_{max}$) estimated from *M*'' peaks at different temperatures vary from 6066.3 Hz ($2.62 \cdot 10^{-5}$ s) to 26084 Hz ($6.10 \cdot 10^{-6}$ s) at 1053 K and 1173 K respectively. The *M*'' peak value increases with increasing temperature and it is indicating that the corresponding value of capacitance decreases with increasing the temperature. The samarium doped cerium thin ceramic films relaxation time were determined at 873 K are $1.17 \cdot 10^{-6}$ s [24]. The relaxation times are higher for Zr-doped $LaNbO_4$ compared to SDC materials because of the lower conductivity which results in smaller number of charge carriers.

According to the Fig. 7, it is seen that the value of the *M*'' peak increases with increasing the temperature and indicating that the corresponding value of capacitance decreases with increasing the temperature. As a subsequence, the maximum of *M*'' is displaced to the lower frequency zone. This relaxation time was estimated from *M*'' and *Z*'' peaks, 2031.6 Hz and 566.98 Hz respectively.

The impedance (*Z*'') vs frequency and electrical modulus (*M*'') vs frequency spectra were used to evaluate the relaxation time (Eq. 2) at different temperatures (Fig. 8). The relaxation time derived from the impedance and the electric modulus is decreasing with the increasing the temperature as well as the concentration of the dopants indicating that the relaxation is enhanced by the impurities.

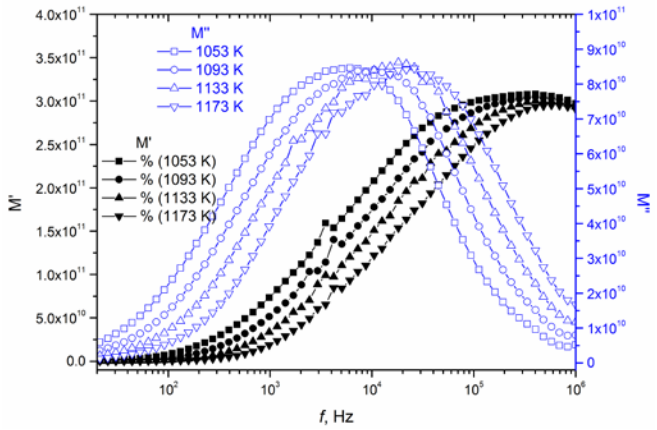


**Fig. 6.** Variation of real part (*M'*) and imaginary part (*M''*) of electric modulus at different temperature for the $LaNb_{1-x}Zr_xO_4$ (Zr 1.14 at. %) thin ceramic films

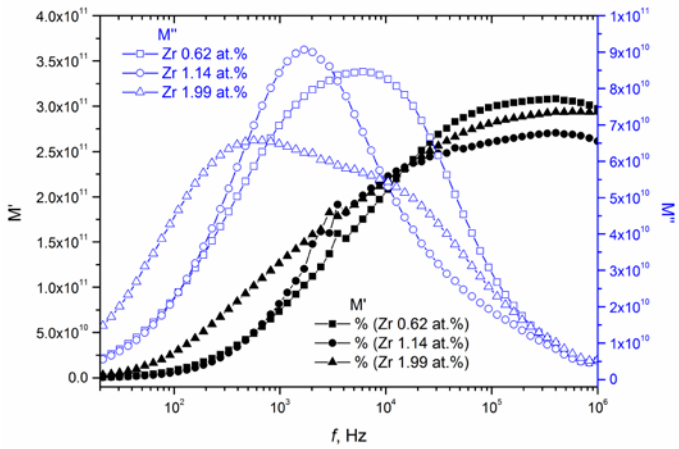


**Fig. 7.** Variation of real part (*M'*) and imaginary part (*M''*) of electric modulus at different concentration at 1053 K temperature

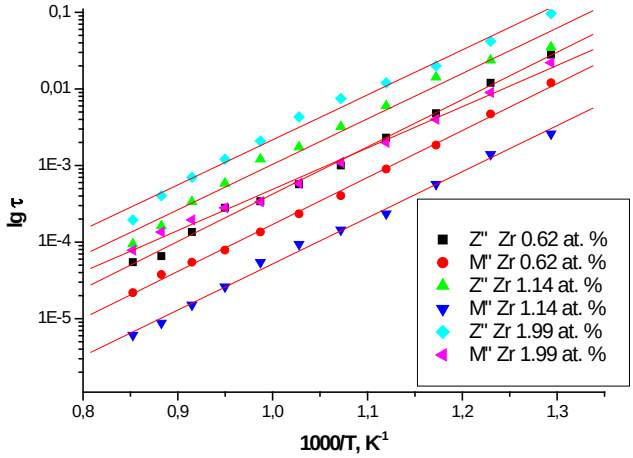


**Fig. 8.** The relaxation times $lg(\tau_{Z''})$ and $lg(\tau_{M''})$ as a function of temperature

The activation energy estimated from impedance and electrical modulus imaginary parts show that by increasing the temperature the capacitance decreases respectively by Arrhenius law. Table 2 summarizes the activation energies estimated using different methods and their average values. It is seen that the activation energies calculated from the slope of the conductivity plot (Fig. 9) are similar to those retrieved from the impedance and electrical modulus. The activation energy estimated from conductivity vs reverse temperature show that the conductivity increases by Arrhenius law.

**Table 2.** Activation energies estimated from the impedance and electrical modulus

| Atomic concentration of Zr in thin film, at. % | Activation energy retrieved from *Z''*, $E_{a1}$, eV | Activation energy retrieved from *M''*, $E_{a2}$, eV | Activation energy from Arrhenius plot, $E_{a3}$, eV | The average activation energy, $E_a$, eV |
|---|---|---|---|---|
| 0.62 | 1.23 | 1.23 | 1.24 | 1.23 |
| 1.14 | 1.18 | 1.20 | 1.19 | 1.19 |
| 1.99 | 1.16 | 1.09 | 1.12 | 1.12 |

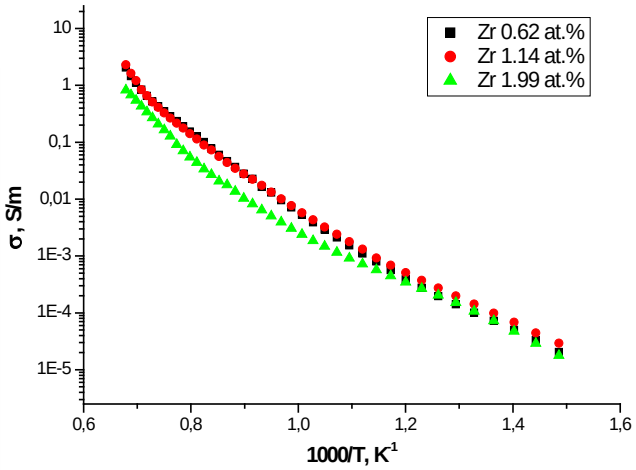


**Fig. 9.** Arrhenius plots for conductivity of $LaNb_{1-x}Zr_xO_4$ thin film

The conductivity plots show different behaviour at lower (below 873 K) and at higher temperature range. The structural relaxation due to the structural inhomogeneities which are seen from the Non-Debye relaxation process influence inadequate Arrhenius behaviour at higher temperature range. Norby et al. [9] determined that the maximum concentration of the dopants is up to 2 % as the higher concentrations cause the formation of the secondary phases in the structure which decrease the conductivity. It is seen that the effect of the dopants is low for the 0.62 % and 1.14 % doped thin films, while the conductivity decrease for 1.99 % doped thin film (Fig. 9). Such behaviour could be explained by the larger grain size in the structure of the formed thin films as could be seen from XRD measurements. The activation energy depends on the Zr concentration and it decreases by increasing the concentration of Zr in the thin films. The lowest activation energy was estimated for the thin ceramic films with Zr dopant concentration equal to 1.99 at. %. The lowest activation energy was estimated to be 1.12 ± 0.01 eV.

## 4. CONCLUSIONS

$LaNb_{1-x}Zr_xO_4$ thin ceramic films were formed by magnetron sputtering technique. It was found that the structure of the formed thin films is nanocrystalline with characteristic XRD peaks corresponding to $LaNbO_4$ tetragonal structure. The Non-Debye type of relaxation is found in the $LaNb_{1-x}Zr_xO_4$ ceramic due to the structural inhomogeneity. The relaxation time as an important

electrical property describing the transitions of the charge carriers was found from *Z''*, *M''* and Cole-Cole plots. It was determined that the relaxation time (from *Z''*) increases as the Zr concentration increases. The relaxation time decreases from $7.84 \cdot 10^{-5}$ s to $2.00 \cdot 10^{-3}$ s with increasing temperature from 773 K to 1173 K for the thin film with Zr concentration equal to 1.99 at %. These thin films distinguished the low activation energy of $E_a$ = 1.12 eV also. The value of activation energy (derived from *Z''(f)* and *M''(f)* functions) is found to be near 1.16 eV and 1.09 eV respectively for Zr 1.99 at. %.

## *Acknowledgments*

This research is funded by the European Social Fund under the Global Grant measure.

**REFERENCES**


1. **Huang, J., Zhou, L., Liang, Z., Gong, F., Han, J., Wang, R.** Promising Red Phosphors $LaNbO_4:Eu^{3+}$, $Bi^{3+}$ for LED Solid-state Lighting Application *Journal of Rare Earths* 28 (3) 2010: pp. 356 – 360. http://dx.doi.org/10.1016/S1002-0721(09)60111-3
2. **Kim, D. W., Kwon, D. K., Yoon, S. H., Hong, K. S.** Microwave Dielectric Properties of Rare-Earth Ortho-Niobates with Ferroelasticity *Journal of the American Ceramic Society* 89 (12) 2006: pp. 3861 – 3864.
3. **Fisher, E. S.** Elastic Moduli and Acoustic Symmetry of Ferroelastic $LaNbO_4$ and $BiVO_4$ *Journal of Physics: Condensed matter* 1 (17) 1989: pp. 2875 – 2890. http://dx.doi.org/10.1088/0953-8984/1/17/009
4. **Magrasó, A., Fontaine, M.-L., Larring, Y., Bredesen, R., Syvertsen, G. E., Lein, H. L., Grande, T., Huse, M., Strandbakke, R., Haugsrud, R., Norby T.** Development of Proton Conducting SOFCs Based on $LaNbO_4$ Electrolyte – Status in Norway *Fuel cells* 11 (1) 2011: pp. 17 – 25.
5. **Masuno, A., Kohara, S., Hannon, A. C., Bychkov, E., Inoue, H**. Drastic Connectivity Change in High Refractive Index Lanthanum Niobate Glasses *Chemistry of Materials* 25 2013: pp. 3056-3061.
6. **Lin, B., Wang, S., Liu, X., Meng, G.** Stable Proton-conducting Ca-doped LaNbO4 Thin Electrolyte-based Protonic Ceramic Membrane Fuel Cells by in Situ Screen Printing *Journal of Alloys and Compounds* 478 (1 – 2) 2009: pp. 355 – 357.
7. **Demin, A. K, Tsiakaras, P. E, Sobyanin, V. A., Hramova, S. Y.** Thermodynamic Analysis of a Methane Fed SOFC System Based on a Protonic Conductor *Solid State Ionics* 152– 153 2002: pp. 555 – 560.
8. **Fontaine, M.-L., Larring, Y., Haugsrud, R., Norby T., Wiink, K., Bredesen, R.** Novel High Temperature Proton Conducting Fuel Cells: Production of $La_{0.995}Sr_{0.005}NbO_4$−electrolyte Thin Films and Compatible Cathode Architectures *Journal of Power Sources* 188 2009: pp. 106 – 113.
9. **Norby, T., Haugsrud, R.** Proton Conduction in Rare-earth Ortho-niobates and Ortho-tantalates *Nature Materials 5* 2006: pp. 193 – 196.
10. **Mokkelbost, T., Lein, H. L., Vullum, P. E., Holmestad, R., Grande, T., Einarsrud, M.-A.** Thermal and Mechanical Properties of $LaNbO_4$-based Ceramics *Ceramics International* 35 2009: pp. 2877 – 2883. http://dx.doi.org/10.1016/j.ceramint.2009.03.041
11. **Mielewczyk-Gryń, A., Gdula, K., Molin, S., Jasinski, P., Kusz, B., Gazda, M.** Structure and Electrical Properties of Ceramic Proton Conductors Obtained with Molten-salt and Solid-state Synthesis Methods *Journal of Non-Crystalline Solids* 356 2010: pp. 1976 – 1979.
12. **Brandao, A. D., Gracio, J., Mather, G. C., Kharton, V. V., Fagg, D. P.** B-site Substitutions in $LaNb_{1-x}M_xO_{4-\delta}$ Materials in the Search for Potential Proton Conductors *Journal of Solid State Chemistry* 184 2011: pp. 863 – 870.
13. **Ivanova, M., Ricote, S., Meulenberg, W. A., Haugsrud, R., Ziegner, M.** Effects of A- and B-site (co-) Acceptor Doping on the Structure and Proton Conductivity of $LaNbO_4$ *Solid State Ionics* 213 2012: pp. 45 – 52. http://dx.doi.org/10.1016/j.ssi.2011.06.012
14. **Fontaine, M.-L., Larring, Y., Haugsrud, R., Norby, T., Wiik, K., Bredesen, R.** Novel High Temperature Proton Conducting Fuel Cells: Production of $La_{0.995}Sr_{0.005}NbO_{4-\delta}$ Electrolyte Thin Films and Compatible Cathode Architectures *Journal of Power Sources* 188(1) 2009: pp. 106-113.
15. **Virbukas, D., Laukaitis, G., Dudonis, J., Milčius, D.** The Properties of Scandium and Cerium Stabilized Zirconium Thin Films Formed by e-beam Technique *Solid State Ionics* 188 2011: pp. 46–49. http://dx.doi.org/10.1016/j.ssi.2010.11.018
16. **Intatha, U., Eitssayeam, S., Wang, J., Tunkasiri, T.** Impedance Study of Giant Dielectric Permittivity in $BaFe_{0.5}Nb_{0.5}O_3$ Perovskite Ceramic *Current Applied Physics* 10 2010: pp. 21–25.
17. **Mokkelbost, T., Kaus, I., Haugsrud, R., Norby, T., Grande, T., Einarsrud, M-A.** High-temperature Proton-Conducting Lanthanum Ortho-niobate-based Materials. Part ii: Sintering Properties and Solubility of Alkaline Earth Oxides. *Journal of American Ceramic Society* 91 2008: pp. 879-886. http://dx.doi.org/10.1016/j.cap.2009.04.006
18. **Syvertsen, G. E., Magraso, A., Haugsrud, R., Einarsrud, M. A., Grande, T.** The Effect of Cation Non-stoichiometry in $LaNbO_4$ Materials *International Journal of Hydrogen Energy* 37 2012: pp. 8017 -8026. http://dx.doi.org/10.1111/j.1551-2916.2007.02232.x
19. **Syvertsen, G. E., Estournès, C., Fjeld, H., Haugsrud, R., Einarsrud, M.-A., Grande, T.** Spark Plasma Sintering and Hot Pressing of Hetero-Doped $LaNbO_4$ *Journal of the American Ceramic Society* 95(5) 2012: pp. 1563-1571. http://dx.doi.org/10.1016/j.ijhydene.2011.10.113
20. **Suman, C. K., Prasad, K., Choudhary, R. N. P.** Complex Impedance Studies on Tungsten-bronze Electroceramic: $Pb_2Bi_3LaTi_5O_{18}$ *Journal of Materials Science* 41 2006: pp 369 – 375. http://dx.doi.org/10.1111/j.1551-2916.2012.05101.x
21. **Shekharam, T., Laxminarasimha, V. R., Yellaiah, G., Kumar, T. M., Nagabhushanam, M.** AC Conductivity, Dielectric and Impedance Studies of $Cd_{0.8-x}Pb_xZn_{0.2}S$ Mixed Semiconductor Compounds *Journal of Alloys and Compounds* 617 2014: pp. 952 – 960. http://dx.doi.org/10.1007/s10853-005-2620-5
22. **Zhao, L. Perry, N. H. Sasaki, K. Bishop, S. R.** Electronic and Ionic Conductivity of $Eu_{0.2}Ce_{0.8}O_{2-\delta}$ *Solid State Ionics* 263 2014: pp. 75 – 79. http://dx.doi.org/10.1016/j.jallcom.2014.08.116
23. **Ramanarayanan, T. A., Worrell, W. L., Tuller, L. H.** Proceedings of the Second International Symposium on Ionic and Mixed Conducting Ceramics *The electrochemical society* NJ USA 1994 ISBN 1-56677-044-0. http://dx.doi.org/10.1016/j.ssi.2014.05.010
24. **Virbukas, D., Sriubas, M., Laukaitis, G.** Structural and Electrical Study of Samarium Doped Cerium Oxide Thin Films Prepared by e-beam Evaporation *Solid State Ionics* 2014 http://dx.doi.org/10.1016/j.ssi.2014.09.036.